Nanophotonic integrated circuits using graphene oxide 2D thin films for nonlinear optics

David J Moss

Nanophotonic integrated circuits using graphene oxide 2D thin films for nonlinear optics

David J. Moss

[a] Optical Sciences Centre, Swinburne University of Technology, Hawthorn, VIC 3122, Australia

ABSTRACT

We report a significant experimental improvement in the performance of all-optical photonic chips that feature ring resonators and nanowires, through the integration of 2D GO (graphene oxide) layered thin films. The films are coated onto SiN, high Hydex glass, and silicon nanowires (SOI), featuring micro-ring resonators (MRRs) and waveguides. We achieve a significantly increased performance in the nonlinear optical performance based on four-wave mixing (FWM) and the Kerr nonlinearity. Our coating method is able to cover large scale areas, using processes that do not require transfer, and with a layer-by-layer coating method. To pattern the devices we use a combination of lift-off with photolithography processes, following processes that are consistent with complementary metal-oxide-semiconductor (CMOS) standards. For the silicon nanowires, we observe large self-phase modulation (SPM) induced spectrum broadening of optical pulses after propagating across SOI nanowires coated in GO induced. Our experimental results show a very large spectral broadening factor (SBF) of a factor of 4.34 for a patterned nanowire containing a film with ten GO layers. We also observe a substantial increase in the nonlinear figure of merit (FOM) of the SOI nanowires, by as much as twenty times, which yields a FOM greater than 5. For the SiN and Hydex waveguides, we observe a significantly increased efficiency in the FWM process by up to 9.1 dB, while in the Hydex waveguides we increase the conversion efficiency by 6.9dB compared to bare waveguides. For the MRRs, we observe an increase in the CE of the FWM process of ~10.3 dB because of resonant enhancement. Our work demonstrates the high capability of GO films to enhance the nonlinear optical performance of ring resonators, waveguides, and nanowires.

Keywords: Kerr nonlinearity, four-wave mixing, nonlinear optics, CMOS compatible photonic chips, graphene oxide

1. INTRODUCTION

The 3rd order nonlinear optical susceptibility has many uses in ultrafast optics, quantum photonics, astronomy, measurement, telecommunications, and others [1-4]. Integrated nonlinear optical chips based on the nonlinear refractive index (Kerr nonlinearity n_2) are capable of much higher speeds compared to electronics, and offer the extra advantages of high stability, low power operation, small footprint, and large scale manufacturing, critical for high bandwidth signal processing and generation for optical communications [5-7].

Whereas silicon nanowires have proven to be an important platform for photonic integrated chips, they suffer from high nonlinear (2 photon absorption TPA) in the 1550nm wavelength range that restricts their performance [5, 6]. Therefore, this has driven the search for new high nonlinearity materials for photonic integrated chips. Other photonic platforms also offer compatibility with complementary metal-oxide-semiconductor (CMOS) fabrication, and these include Hydex [8, 9] as well as SiN [10, 11]. Both of these have negligible TPA in the telecom band, but unfortunately they also degrade their nonlinear performance because of their much lower 3rd order nonlinear response. To overcome this, layered 2D graphene oxide (GO) films have attracted a lot of interest – more than most 2D materials – because of its facile methods of fabrication as well as the ability to tune its properties [12-20]. Recently, we demonstrated GO films that exhibited a very large nonlinear Kerr optical susceptibility that is four to five orders of magnitude larger than Si and a further order of magnitude larger than SiN. [16] We reported greatly increase efficiency for four wave mixing (FWM) in microring resonators (MRRs) and doped silica waveguides with integrated GO films [21, 22]. Here, we demonstrate enhanced 3rd order all-optical response in SiN waveguides [24] and silicon nanowires [23], both using 2D layered films of GO. Because of the very high light-matter overlap between the highly nonlinear GO films and the integrated waveguides, our results for self-phase modulation (SPM) measurements show significantly enhanced spectral broadening in patterned GO coated SOI nanowires. The dependence of the Kerr nonlinearity of the GO films on the number of film layers as well as the optical pulse intensity reveals very interesting trends leading to physical insights. The GO films evolve from 2D monolayer like behaviour to quasi-bulk behavior. We observe very substantially increased nonlinear optical response for the hybrid GO waveguides in comparison to uncoated waveguides. We obtain a nonlinear parameter for the silicon nanowires coated in GO that is enhance by up to a factor of 16 times, and more importantly, with a figure of merit (FOM) that is more than 20 x higher, yielding a nonlinear FOM greater than 5. We obtain a FWM conversion efficiency (CE) that is enhanced by $\approx$6.8dB for a Hydex waveguide uniformly coated with 2 GO layers and

an increase of ≈9.2 dB for a silicon nitride waveguide patterned with five GO layers. We observe an enhancement of up to ~10.3 dB in the FWM conversion efficiency for GO coated MRRs. Our results indicate the strong ability of 2D GO films to enhance the nonlinear optical performance of CMOS compatible photonic platforms.

2. INCREASED KERR NONLINEARITY IN SILICON NANOWIRES COATED WITH GO

Fig. 1a illustrates a GO film integrated with an SOI nanowire waveguide. The SOI nanowire fabrication can be done using either e-beam lithography or deep ultraviolet photolithography to achieve the patterning. The devices are then etched using inductively coupled plasma enhanced processes. All of our processes are compatible with well established fabrication methods used for silicon chips [25, 26]. The thickness of the GO films was about two nanometers per layer [23]. The deposition of the layers was accomplished with a solution based method to achieve single layer at a time fabrication [20, 21, 27]. In comparison to the elaborate procedures that are typically used to transfer many 2D materials including TMDCs and graphene [28, 29], our approach results in film coatings that are conformal and achieved without the need for transfer processes. Furthermore, it results in high repeatability, extremely robust adherence of the film to the surface of the photonic chip, greatly enhanced fabrication stability, and finally the ability to precisely control the thickness of the films as well as the layer number [30].
Figure 1b illustrates a silicon chip fabricated with a 400 micron long window. Aside from enabling the accurate control and placement of the GO film coating length contacted to the nanowires, the openings also allowed us to measure devices with much shorter lengths of GO films and with a much greater thickness – up to twenty layers. This offered much greater degree of control to engineer the SPM spectral broadening performance. Figure 1c shows a scanning electron microscope picture of a silicon nanowire conformally coated with one GO layer. Note that the fact that the GO layers were coated conformally on both the top and sides of the nanowires differs from our previous work where the Hydex devices were coated with GO layers on only the waveguide top [30, 31]. In comparison to the low index contrast, large mode field size doped silica waveguides, the SOI nanowires studied here yielded a much larger overlap between the GO film and the optical field extending from the waveguide. This is important for enhancing the nonlinearity for FWM, SPM and other processes. Fig. 1(d) illustrates devices integrated with GO films together with the Raman spectra showing the G (1590 cm-1) peaks and D (1345 cm-1) peaks arising from the GO. The SOI chip was coated with GO 5 layers. Microscope images before and after GO coating of the same SOI chip are shown in the insets, indicating high quality film morphology.

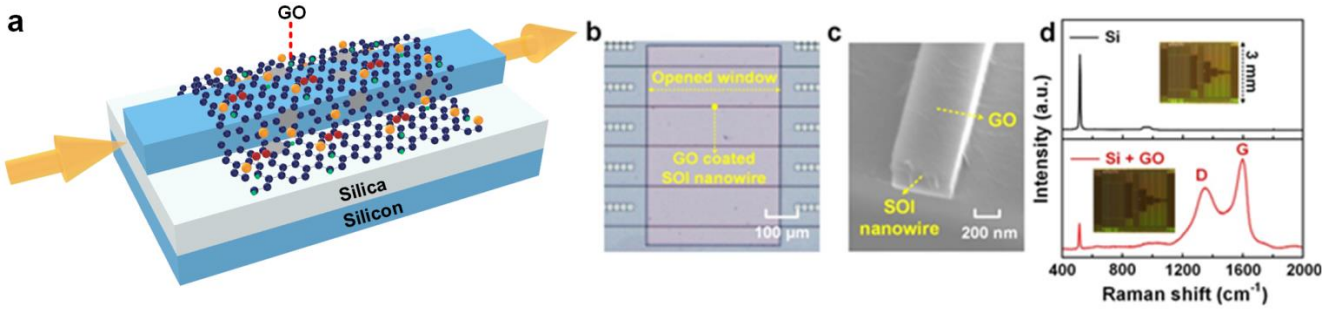

Figure 1. (a) Schematic diagram of a SOI nanowire coated with a GO film. (b) Optical image of a silicon waveguide with a 400 micron opened window in the upper cladding coated with a GO film. (c) SEM (scanning electron microscope) image of a conformally coated SOI nanowire for 1 GO layer (d) Raman spectra of a Si device with no GO and five GO layer. Insets show the corresponding microscope images.

Figure 2 shows the experiments for the SPM measurements, including the normalized spectra (Figure 2a-i) of the input and output pulses after propagatin across 2.2-mm-long SOI nanowires containing one to three GO layers, as well as the corresponding bare nanowire output optical spectrum. All of the measurements had pulses of energy ~51.5 pJ (peak power ~13.2 W) coupled into the waveguides. In comparison to the pulse input spectrum, after transmission across the uncoated nanowire, the output spectrum displayed significant SPM broadening. This was expected because of silicon's large Kerr optical nonlinearity. The GO coated silicon devices, in contrast, showed much greater SPM broadening in the spectra relative to the uncoated devices, reflecting the significantly increased nonlinear suspeptibility of the coated devices. Figure 2a-ii illustrates the analogous measurements for the silicon devices having a length of 400 microns with five to twenty GO layers. These measurements used the same optical pulse energy as that used in the measurements shown in Figure 2a-i. Devices that contained short lengths of GO films but having a larger thickness clearly display higher SPM broadening compared to the uncoated devices. In s Figures 2a-i and 2a-ii, the largest SPM broadening is obtained for waveguides having an intermediate number of layers of GO - 10 and 2 GO layers in a-ii and a-i, respectively. This results from a trade-off intrinsic to enhancing the nonlinear Kerr response that is dominant in devices having short lengths of GO films, while mitigating the increase in linear loss that becomes larger as the waveguide length increases.

After transmission through the nanowires, the output spectra of the pulses (Figures 2b-i and b-ii) show that the spectra increase in SPM broadening with input pulse power. The experiments were performed with devices having (i) two and (ii) ten GO film layers. The optical pulse spectra were measured at the output for ten pulse energies, varying from ~8.2 to ~51.5 pJ (coupled energy), corresponding to optical peak pulse powers ranging from ~2.1 to ~13.2 W (in-waveguide). As we expect, with increasing pulse energy, the output pulse SPM broadening also increased, and with a measurable spectral asymmetry due mainly to free-carriers generated in the silicon, creating both free carrier dispersion (FCD) and absorption (FCA). Since the free carrier response time is much longer than the optical pulse, the influence of the FCA on the shape of the pulse is delayed, and this creates the asymmetry in the output optical pulse spectrum. FCD induced by FCA increases the asymmetry further.

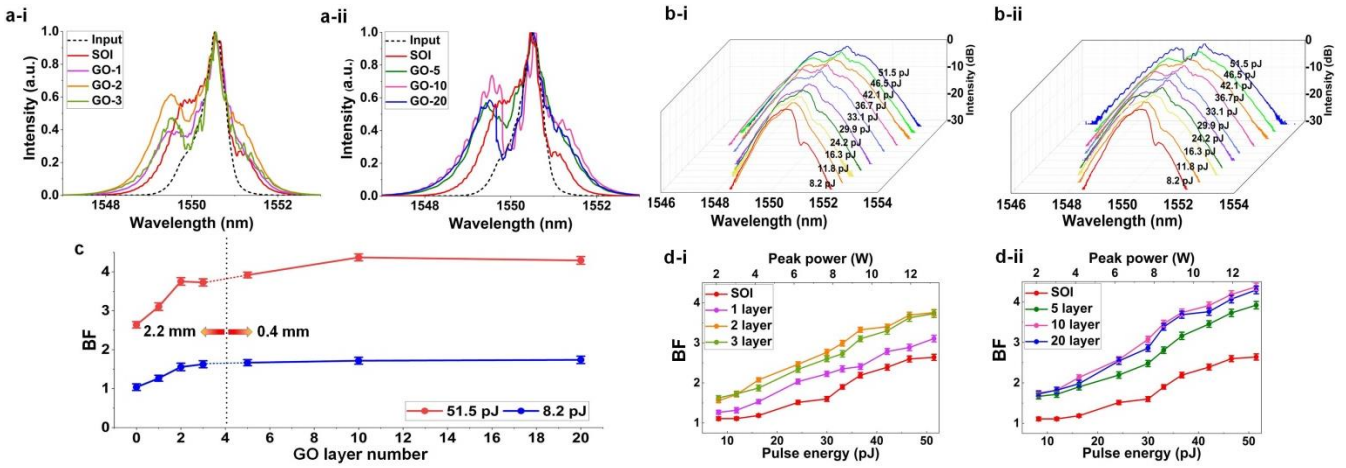

Figure 2. Results of the SPM experiments. (a) pulse optical spectra before and after propagation across the GO-coated silicon nanowires with a pulse energy of ~51.5 pJ (coupled). (b) Spectra of the optical pulses for a range of pulse energies for SOI nanowires coated in GO films. (c) Output spectra BFs taken for a range of different numbers of GO layers, all with constant pulse energies of 8.2 and 51.5 pJ (coupled). (d) Measured BFs of the pulse spectra for different pulse energies. In (a), (b) and (d), the graphs shown in (i) and (ii) illustrate the measurements for 2.2-mm-long silicon devices having one to three GO layers and for a 400 micron long coating with five to twenty GO layers, respectively. For comparison, in (a), (c) and (d), the measurements obtained with uncoated SOI nanowires are also shown.

To quantitively analyze the output SPM broadening, we define a broadening factor (BF - the square of the pulse RMS spectral width at the waveguide output facet normalized to the input [31]). Figure 2c shows the measured output pulse spectra BFs after propagation across uncoated nanowires along with coated devices, for pulse energies 8.2 and 51.5 pJ. The coated silicon nanowires exhibited larger BFs compared to uncoated devices, while the BFs measured with a (coupled) pulse energy of 51.5 pJ are larger than the results measured for pulse energies of 8.2 pJ. This is in agreement with the measurements shown Figs 2a and 2b. For a pulse energy of 51.5 pJ, we obtain BFs as high as 3.75 to 4.34 for devices having two and ten layers of GO, respectively. These results agree with those shown in Fig. 2a – where the greatest SPM broadening occurred for devices having an intermediate number of film layers. Again, this was a result of the intrinsic trade-off between enhancing the nonlinear Kerr response and minimizing the increase in linear loss. The SPM BFs of the output pulse spectra as a function of pulse energy are illustrated in Figs. 2d-ii and 2d-i for silicon devices with 5−20 GO and 3 layers of GO, respectively. This indicates that the SPM BF increases as the pulse energy increases, and indicates a larger SPM broadening in agreement with the measurements shown in Fig. 2b.

3. INCREASED FWM EFFICIENCY SIN AND HYDEX WAVEGUIDES COATED WITH GO

The Hydex waveguides [5] (Fig. 3a) coated with GO films had a 2 × 1.5 μm cross section. The waveguide is clad by silica with the top cladding removed to allow coating the waveguide with GO films. The GO films have a thickness of 2 nm per layer, and integrated on top of the waveguide to enhance the optical overlap of the mode with the GO film. The GO Kerr nonlinearity is 10^{-15} to 10^{-14} m^2/W [16, 19], somewhat less than graphene, which is 10^{-13} m^2/W [19, 32, 33], but nevertheless is much larger than Hydex, at 10^{-19} m^2/W, or silica, which is 10^{-20} m^2/W [5]. The devices were produced with processes that were compatible with CMOS standards [34, 35]. Doped silica high-index glass films (n = ~1.60 at 1550 nm) were first grown using PECVD, followed by patterning using stepper mask aligners. They were then etched using reactive ion etching (RIE) to fabricate the waveguides that featured very low surface roughness. Next, silica glass (n = ~1.44 at 1550 nm) was deposited via PECVD and the waveguide upper cladding removed by chemical mechanical polishing (CMP). Finally, the GO film was deposited on top of the waveguide using a solution-based approach that enables layer-by-layer deposition of GO films [20]. Fig. 3b shows a picture of a waveguide having 2 GO layers GO, clearly showing that the surface quality is good, resulting in relatively low

loss. The presence of GO on the waveguide is confirmed by Raman spectroscopic measurements (Figure 3c) that show the representative D (1345 cm^{-1}) and G (1590 cm^{-1}) peaks of GO [16].

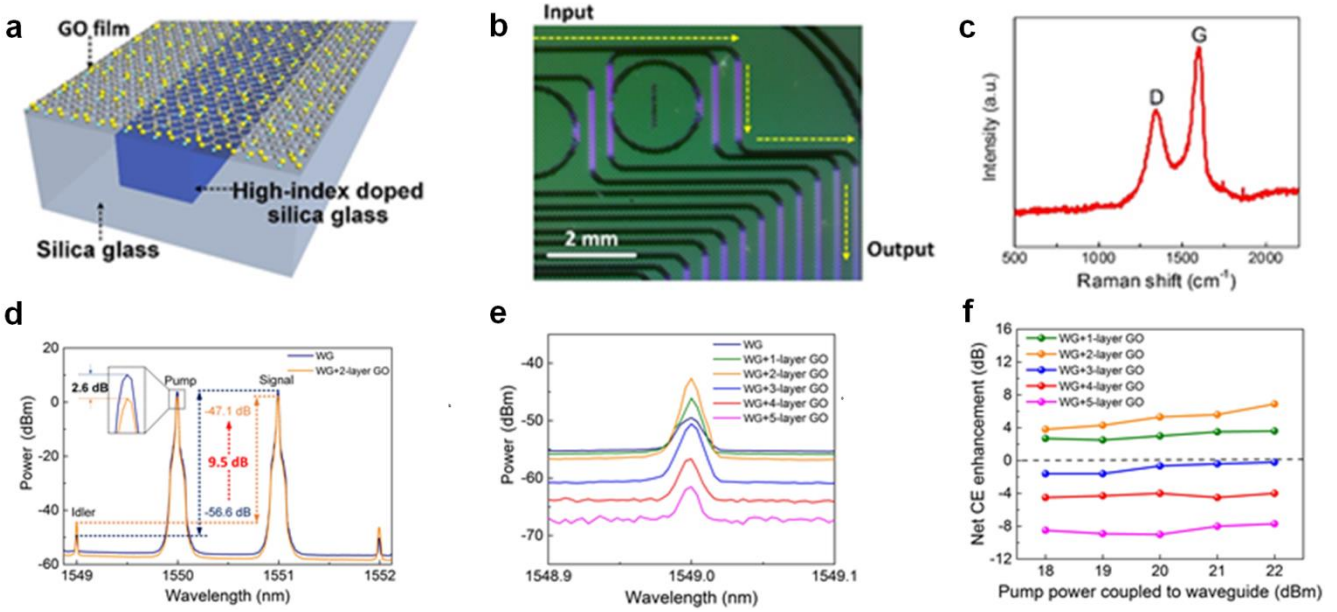

Figure 3. (a) Diagram and (b) Photo of the Hydex waveguides coated with GO films. (c) Raman spectra taken from the chip coated in GO. (d) waveguide FWM spectra for devices without GO and two GO layers. (e) idler spectra from the FWM process in the devices coated with 0 to 5 GO layers. (f) Overall enhancement in the CE for a range of coupled pump powers, for 1 to 5 GO layers.

Figure 3d shows the FWM results from an uncoated waveguide that is 1.5 cm in length and with 2 GO layers. The power of the pump was kept constant at 1W input and ~ 22 dBm coupled into the waveguide. Even though the propagation loss of the coated device increased by ~2.6 dB, it nonetheless yielded higher output idler powers relative to uncoated waveguides. The conversion efficiency (CE, defined as the ratio of the idler output power to the output signal power , i.e., $P_{out,\ idler}/P_{out,\ signal}$) of the waveguide with and without GO were ~-47.1 dB and ~-56.6 dB, respectively, corresponding to a CE enhancement of ~9.5 dB. After accounting for the increase in propagation loss, the resulting enhancement in the CE, which is defined as the increase idler output power at a fixed input pump power, was 6.9 dB. Figure 3e shows the idler spectra (input pump power 22 dBm) for the devices coated with one to five GO layers. For the device coated with one and two GO layers, an overall enhancement in the CE resulted. For devices having more than two GO layers, the CE became smaller, resulting from the supra-linear increase in propagation loss as a function of the number of GO layers. The idler output powers as a function of pump power for the bare devices and for two GO layers are illustrated in Fig. 3f.

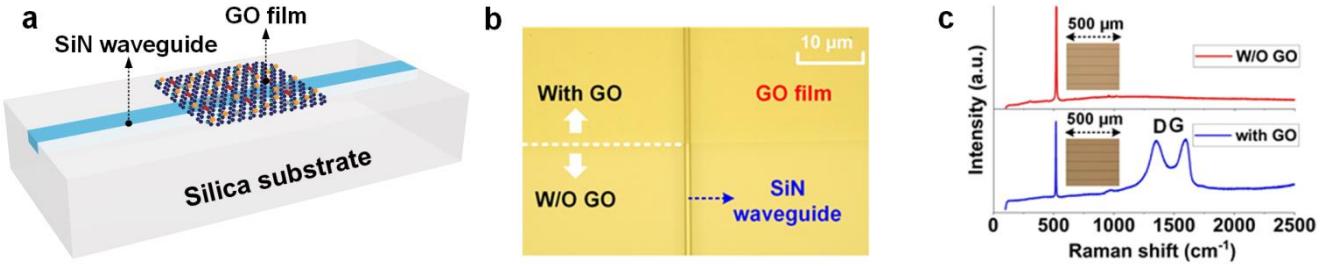

Figure 4. (a) Diagram of silicon nitride waveguide coated with GO. (b) Photo image of a silicon nitride waveguide patterned with 10 GO layers. (c) silicon nitride chip Raman spectra with no GO and 10 GO layers. Insets: related images from microscope.

Figure 4a shows the SiN waveguide (cross section 1.6 μm × 0.66 μm) integrated with a GO film. The waveguides were fabricated using an annealing-free and crack-free CMOS compatible process [36, 37]. A silicon nitride layer was first deposited using LPCVD in two stages, each depositing 370nm layers so as to minimize stress and avoid cracking. To deposit top quality films, we used extremely low growth rates at less than two nanometers per minute. We then fabricated waveguides by patterning with deep UV stepper mask photolithography and fluorine dry etching that produces very small surface roughness. We then deposited a 3μm upper cladding composed of silica using high-density PECVD to prevent formation of voids. To enhance the optical mode field overlap with the GO films, the silica upper cladding was removed with highly selective CMP, with very little etching of the silicon nitride and little remaining topography. A microscope photo of a silicon nitride waveguide

patterned with ten layers of GO (Fig. 4b) shows the high films morphology and transmittance. Scanning electron microscope images of GO films having as high as five layers of GO (Fig. 4b), clearly illustrated the layered nature of the film. The Raman spectra of a silicon nitride chip with no films and with ten uniformly coated GO layers (Figure 4c) clearly indicate the successful incorporation of the GO films because of the presence of the G (1590 cm-1) and D (1345 cm-1) resonances.

FWM measurements are shown in Fig. 5 for the uncoated and uniformly coated (one and two GO layers) silicon nitride devices (Figure 5a-i). The power remained constant at 200mW for both signal and pump at the device input, equating to 18 dBm coupled power. The variation in the spectra baselines is a result of the different propagation losses for the devices. Although the hybrid waveguide with 1 layer of GO had an increased propagation loss of ≈7.1 dB, it clearly displays an increased idler output power relative to uncoated waveguides. The CE of the SiN devices for one GO layer and the uncoated device were -58.4 dB and -65.7 dB, respectively, reflecting an enhancement of the CE of 7.3 dB relative to the bare device. In contrast to the net enhancement in the CE enhancement for the coated devices with one GO layer, the devices coated with two GO layers had a lower CE.

The FWM spectra for the SiN devices having five and ten layers of patterned GO films are shown in Fig. 5a-ii. The coupled CW signal and pump powers were both 18 dBm, as for Fig. 5a-i. The devices with patterned films had a larger insertion loss than bare waveguides, whereas waveguides coated with both five and ten layers of GO layers resulted in an increase in the idler output power. We measured the largest increase in the CE at 9.1 dB for devices patterned with five GO layers, which is even larger than the uniformly coated device with 1 layer of GO. This arises due to the intrinsic balance between enhancing the efficiency of the FWM process, that is largest for devices patterned with short GO films, and minimizing the loss that is largest for the long uniformly coated devices. Figure 5b illustrates the measured CE as a function of pump power for the patterned and uniformly coated devices, where the results shown are an average of 3 measurements for every sample. With increasing pump power , the CE linearly increased without any sign of saturating behaviour for the uncoated SiN and coated waveguides, reflecting the low TPA in both coated and uncoated SiN waveguides. For the uncoated devices, the variation in CE with pump power is almost linear, with a slope of around 2 as predicted by theory [38]. For the coated devices, the dependence of CE on input power deviated slightly from linear, again with a slope near two, but which increased for larger powers. Figure 5c compares the CE of the bare devices for four different GO layer numbers (1, 2, 5, and 10), where it is evident that devices coated with an in-between number of GO layers had the largest CE. Again, this was due to the balance between increasing the nonlinearity γ and minimizing the loss in the coated devices – both of these get larger as the number of GO layers increases.

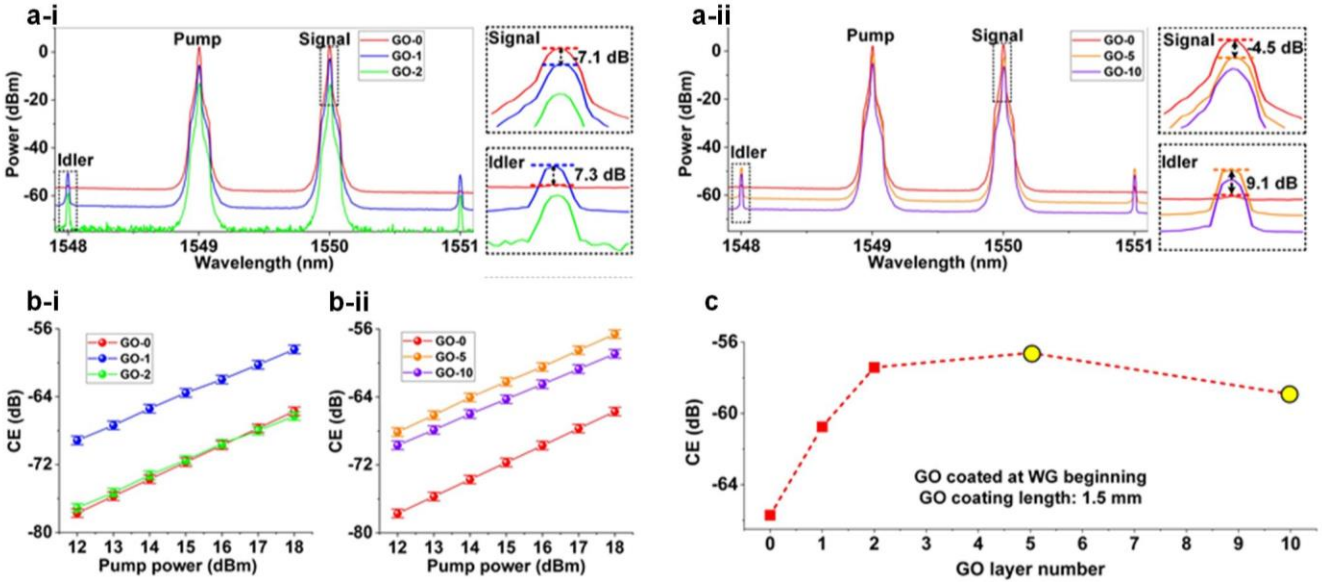

Figure 5. Results for the FWM experiments. (a) optical spectra. Insets illustrate a zoom-in near the idler and signal. (b) CE as a function of coupled pump power. In (a) and (b), graph (i) reflects the measurements for SiN devices coated uniformly with one and two GO layers while graph (ii) indicates the results for SiN devices patterned with five and ten GO layers. (c) Theoretical CE versus number of GO layers. In (c), the measurements for uncoated SiN devices are also shown as a reference. The coating length is 1.5 mm and GO coating position is near the waveguide beginning.

4. FWM IN INTEGRATED RING RESONATORS WITH GO FILM COATINGS

The MRR integrated with the GO film (Figure 6a) was fabricated in high index doped silica glass with CMOS compatible processes [8, 39] using chemical mechanical polishing (CMP) as the final process to planarize and remove the upper cladding in order to coat the top of the waveguide surface with the GO film. High index doped silica glass has been extremely successful as an integration platform for nonlinear optics because of its extremely low linear loss and together with its negligible nonlinear loss [9, 40, 41]. Its Kerr coefficient n_2 (~1.3×10^{-19} m^2/W) is admittedly lower than that of silicon (~4.5×10^{-18} m^2/W), but this is more than compensated for by its negligible nonlinear loss even at extremely high light intensities, resulting in an essentially infinite nonlinear figure of merit (>>1), or at any rate much higher than silicon, which is about FOM ~0.3 [5]. Figure 6b shows microscope photos of a MRR with 50 patterned GO layers of length 50 μm. We mention that, of the 9 concentric rings, only the central on was connected to the drop or through bus nanowires − the rest were included just to assist in alignment. The Raman spectra of the devices with no GO and with 2 layers of uniformly coated GO film are shown in Fig. 6c. The successful integration of the GO film onto the top surface is confirmed by the representative D (1345 cm-1) and G (1590 cm-1) GO peaks.

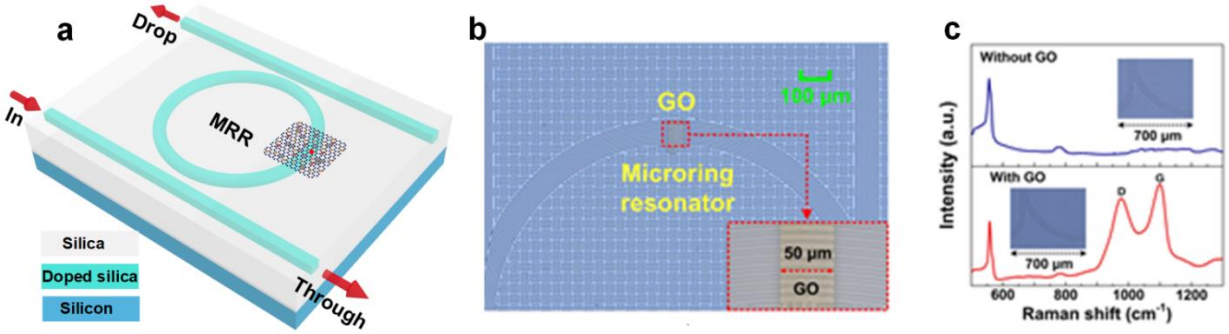

Figure 6. (a) Diagram of MRR coated with GO. Inset: GO atomic structure. (b) Microscopic photo of an integrated MRR coated with 50 patterned GO layers. Inset shows zoom-in view of the patterned GO film. (c) Raman spectra of a device with no GO and with 2 layers of GO. Inset: microscope photo images.

The FWM spectra of the uniformly coated and MRRs with 1−5 GO layers along with the uncoated MRR are shown in Figure 7a. We kept the coupled pump power constant at ~22 dBm coupled inside the MRRs, with factoring out the extra propagation loss of the input bus waveguide induced by the GO film as well as the coupling loss from the input SMF array to the input bus waveguide. The signal and pump had equal power and separated in wavelength by two MRR FSRs. The GO-coated MRRs had an excess insertion loss relative to the uncoated MRRs, whereas the MRRs coated with one and two GO layers clearly indicate larger idler powers. The MRR CE for uncoated devices and with one GO layer were ~ -48.4 dB, ~ -40.8 dB, respectively, yielding an enhancement in the CE of 7.6 dB for the coated device. The FWM spectra of the MRRs for 10−50 GO layers patterned with a length of ~50 μm, and for an input pump power of 22 dBm (as in Figure 7a) are shown in Figure 7b. The patterned MRRs also had an increase in insertion loss relative to the uncoated devices. All coated devices displayed an increased idler power. The CE increased with a maximum of ~10.3 dB for a ring resonator with 50 patterned GO layers. The increase in CE enhancement and insertion loss obtained from Figs 7a,b are displayed in Figs. 7c,d. It is evident that the increased insertion loss gets larger with increasing numbers of GO layers. For the MRRs that are coated uniformly, the relative increase in CE becomes less with fewer number of GO layers, while the patterned MRRs show the reverse behaviour. This could result from the balancing between increasing the FWM efficiency, that is largest for MRRs having short patterned GO film lengths, and minimizing the overall linear loss, that is largest for uniformly coated MRRs.

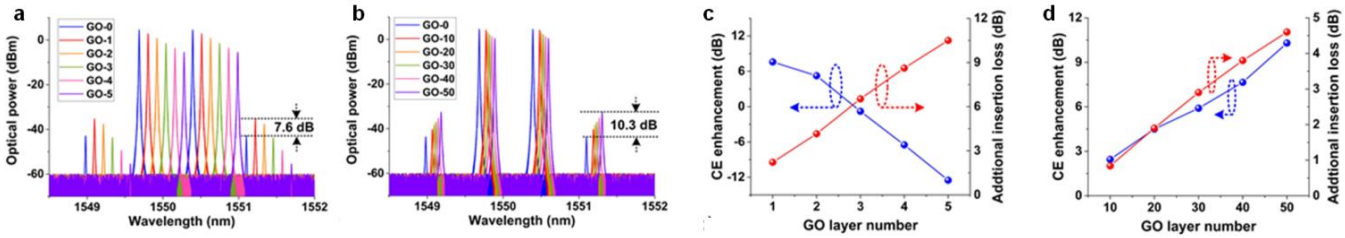

Figure 7. (a)−(b) Optical spectra of FWM at a pump power of 22 dBm for the MRRs with 1−5 layers of uniformly coated and 10−50 layers of patterned GO films, respectively. (c)−(d) CE enhancement and additional insertion loss extracted from (a) and (b), respectively. In (a) and (b), the results for uncoated MRR (GO-0) are also shown for comparison.

5. CONCLUSION

We report increased efficiency for third-order nonlinear optics based on the Kerr nonlinearity and FWM in ring resonators, nanowires, and waveguides integrated with 2D layered GO films. We obtain precise control of the thickness, length, and placement, of the GO films through the use of a layer-by-layer GO film coating process together with photolithography and lift-off processes. Because of the strong overlap between the GO films and the optical mode, we obtain a high nonlinear parameter for SOI nanowires coated with GO films – achieving up to 16x higher nonlinearity together with an increased nonlinear FOM by as much as 20 times. In addition, we see a significant increase in the CE of the FWM process of $\approx$6.1 dB Hydex device coated uniformly with two GO layers and $\approx$9.1 dB for a SiN device patterned with GO films having five layers. We obtain as high as ~10.3 dB enhancement in the four wave mixing conversion efficiency for the MRRs. Calculations show that our results can be significantly advanced [42-47] particularly with improved techniques of integration. [48] This work will is relevant for integrated microcomb devices and their application to new technologies. [49-169] In conclusion, this work verifies the ability to greatly increase the nonlinear device performance of waveguides, ring resonators, and nanowires by incorporating them with layered 2D graphene oxide films.

The authors declare that we have no competing interests.

REFERENCES

[1] S. T. Cundiff, "Metrology - New generation of combs," *Nature,* vol. 450, no. 7173, pp. 1175-1176, Dec 20, 2007.

[2] A. Pasquazi, M. Peccianti, L. Razzari, D. J. Moss, S. Coen, M. Erkintalo, Y. K. Chembo, T. Hansson, S. Wabnitz, P. Del'Haye, X. Xue, A. M. Weiner, and R. Morandotti, "Micro-combs: A novel generation of optical sources," *Physics Reports,* vol. 729, pp. 1-81, 2018.

[3] H. Guo, C. Herkommer, A. Billat, D. Grassani, C. Zhang, M. H. P. Pfeiffer, W. Weng, C.-S. Brès, and T. J. Kippenberg, "Mid-infrared frequency comb via coherent dispersive wave generation in silicon nitride nanophotonic waveguides," *Nature Photonics,* vol. 12, no. 6, pp. 330-335, 2018.

[4] E. A. Kittlaus, H. Shin, and P. T. Rakich, "Large Brillouin amplification in silicon," *Nature Photonics,* vol. 10, no. 7, pp. 463-467, 2016.

[5] D. J. Moss, R. Morandotti, A. L. Gaeta, and M. Lipson, "New CMOS-compatible platforms based on silicon nitride and Hydex for nonlinear optics," *Nature Photonics,* vol. 7, no. 8, pp. 597-607, 2013/08/01, 2013.

[6] J. Leuthold, C. Koos, and W. Freude, "Nonlinear silicon photonics," *Nature Photonics,* vol. 4, no. 8, pp. 535-544, 2010/08/01, 2010.

[7] T. J. Kippenberg, A. L. Gaeta, M. Lipson, and M. L. Gorodetsky, "Dissipative Kerr solitons in optical microresonators," *Science,* vol. 361, no. 6402, pp. 567-+, Aug 10, 2018.

[8] M. Ferrera, L. Razzari, D. Duchesne, R. Morandotti, Z. Yang, M. Liscidini, J. E. Sipe, S. Chu, B. E. Little, and D. J. Moss, "Low-power continuous-wave nonlinear optics in doped silica glass integrated waveguide structures," *Nature Photonics,* vol. 2, no. 12, pp. 737-740, 2008/12/01, 2008.

[9] L. Razzari, D. Duchesne, M. Ferrera, R. Morandotti, S. Chu, B. E. Little, and D. J. Moss, "CMOS-compatible integrated optical hyper-parametric oscillator," *Nature Photonics,* vol. 4, no. 1, pp. 41-45, 2010/01/01, 2010.

[10] M. H. P. Pfeiffer, A. Kordts, V. Brasch, M. Zervas, M. Geiselmann, J. D. Jost, and T. J. Kippenberg, "Photonic Damascene process for integrated high-Q microresonator based nonlinear photonics," *Optica,* vol. 3, no. 1, pp. 20-25, 2016/01/20, 2016.

[11] J. S. Levy, A. Gondarenko, M. A. Foster, A. C. Turner-Foster, A. L. Gaeta, and M. Lipson, "CMOS-compatible multiple-wavelength oscillator for on-chip optical interconnects," *Nature Photonics,* vol. 4, no. 1, pp. 37-40, 2010/01/01, 2010.

[12] K. P. Loh, Q. Bao, G. Eda, and M. Chhowalla, "Graphene oxide as a chemically tunable platform for optical applications," *Nature Chemistry,* vol. 2, no. 12, pp. 1015-1024, 2010/12/01, 2010.

[13] X. Li, H. Ren, X. Chen, J. Liu, Q. Li, C. Li, G. Xue, J. Jia, L. Cao, A. Sahu, B. Hu, Y. Wang, G. Jin, and M. Gu, "Athermally photoreduced graphene oxides for three-dimensional holographic images," *Nature Communications,* vol. 6, no. 1, pp. 6984, 2015/04/22, 2015.

[14] X. Zheng, B. Jia, H. Lin, L. Qiu, D. Li, and M. Gu, "Highly efficient and ultra-broadband graphene oxide ultrathin lenses with three-dimensional subwavelength focusing," *Nature Communications,* vol. 6, no. 1, pp. 8433, 2015/09/22, 2015.

[15] H. Lin, B. C. P. Sturmberg, K.-T. Lin, Y. Yang, X. Zheng, T. K. Chong, C. M. de Sterke, and B. Jia, "A 90-nm-thick graphene metamaterial for strong and extremely broadband absorption of unpolarized light," *Nature Photonics,* vol. 13, no. 4, pp. 270-276, 2019/04/01, 2019.

[16] X. Zheng, B. Jia, X. Chen, and M. Gu, "In Situ Third-Order Non-linear Responses During Laser Reduction of Graphene Oxide Thin Films Towards On-Chip Non-linear Photonic Devices," *Advanced Materials,* vol. 26, no. 17, pp. 2699-2703, 2014/05/01, 2014.

[17] K.-T. Lin, H. Lin, T. Yang, and B. Jia, "Structured graphene metamaterial selective absorbers for high efficiency and omnidirectional solar thermal energy conversion," *Nature Comm.,* vol. 11, no. 1, pp. 1389, 2020/03/13, 2020.

[18] J. Wu, L. Jia, Y. Zhang, Y. Qu, B. Jia, and D. J. Moss, "Graphene Oxide for Integrated Photonics and Flat Optics," *Advanced Materials,* Vol. 33 (3) 2006415 (2021). DOI:10.1002/adma.202006415.

[19] X. Xu, X. Zheng, F. He, Z. Wang, H. Subbaraman, Y. Wang, B. Jia, and R. T. Chen, "Observation of Third-order Nonlinearities in Graphene Oxide Film at Telecommunication Wavelengths," *Scientific Reports,* vol. 7, no. 1, pp. 9646, 2017/08/29, 2017.

[20] Y. Yang, H. Lin, B. Y. Zhang, Y. Zhang, X. Zheng, A. Yu, M. Hong, and B. Jia, "Graphene-Based Multilayered Metamaterials with Phototunable Architecture for on-Chip Photonic Devices," *ACS Photonics,* vol. 6, no. 4, pp. 1033-1040, 2019/04/17, 2019.

[21] Y. Yang, J. Wu, X. Xu, Y. Liang, S. T. Chu, B. E. Little, R. Morandotti, B. Jia, and D. J. Moss, "Invited Article: Enhanced four-wave mixing in waveguides integrated with graphene oxide," *APL Photonics,* vol. 3, no. 12, pp. 120803, 2018/12/01, 2018.

[22] J. Wu, Y. Yang, Y. Qu, L. Jia, Y. Zhang, X. Xu, S. T. Chu, B. E. Little, R. Morandotti, B. Jia, and D. J. Moss, "2D Layered Graphene Oxide Films Integrated with Micro-Ring Resonators for Enhanced Nonlinear Optics," *Small,* vol. 16, no. 16, pp. 1906563, 2020/04/01, 2020.

[23] Y. Zhang, J. Wu, Y. Yang, Y. Qu, L. Jia, T. Moein, B. Jia, and D. J. Moss, "Enhanced Kerr Nonlinearity and Nonlinear Figure of Merit in Silicon Nanowires Integrated with 2D Graphene Oxide Films," *ACS Applied Materials & Interfaces,* vol. 12, no. 29, pp. 33094-33103, 2020/07/22, 2020.

[24] Y. Qu, J. Wu, Y. Yang, Y. Zhang, Y. Liang, H. El Dirani, R. Crochemore, P. Demongodin, C. Sciancalepore, C. Grillet, C. Monat, B. Jia, and D. J. Moss, "Enhanced Four-Wave Mixing in Silicon Nitride Waveguides Integrated with 2D Layered Graphene Oxide Films," *Advanced Optical Materials,* Vol. 8 (21) 2001048, 2020. DOI: 10.1002/adom.202001048.

[25] W. Bogaerts, and L. Chrostowski, "Silicon Photonics Circuit Design: Methods, Tools and Challenges," *Laser & Photonics Reviews,* vol. 12, no. 4, pp. 1700237, 2018/04/01, 2018.

[26] A. Autere, H. Jussila, Y. Dai, Y. Wang, H. Lipsanen, and Z. Sun, "Nonlinear Optics with 2D Layered Materials," *Advanced Materials,* vol. 30, no. 24, pp. 1705963, 2018/06/01, 2018.

[27] J. Wu, Y. Yang, Y. Qu, X. Xu, Y. Liang, S. T. Chu, B. E. Little, R. Morandotti, B. Jia, and D. J. Moss, "Graphene Oxide Waveguide and Micro-Ring Resonator Polarizers," *Laser & Photonics Reviews,* vol. 13, no. 9, pp. 1900056, 2019/09/01, 2019.

[28] L. Liu, K. Xu, X. Wan, J. Xu, C. Y. Wong, and H. K. Tsang, "Enhanced optical Kerr nonlinearity of MoS_2 on silicon waveguides," *Photonics Research,* vol. 3, no. 5, pp. 206, 2015.

[29] Q. Feng, H. Cong, B. Zhang, W. Wei, Y. Liang, S. Fang, T. Wang, and J. Zhang, "Enhanced optical Kerr nonlinearity of graphene/Si hybrid waveguide," *Applied Physics Letters,* vol. 114, no. 7, pp. 071104, 2019/02/18, 2019.

[30] G. Cao, H. Lin, S. Fraser, X. Zheng, B. Del Rosal, Z. Gan, S. Wei, X. Gan, and B. Jia, "Resilient graphene ultrathin flat lens in aerospace, chemical, and biological harsh environments," *ACS applied materials & interfaces,* vol. 11, no. 22, pp. 20298-20303, 2019.

[31] P. Demongodin, H. El Dirani, J. Lhuillier, R. Crochemore, M. Kemiche, T. Wood, S. Callard, P. Rojo-Romeo, C. Sciancalepore, C. Grillet, and C. Monat, "Ultrafast saturable absorption dynamics in hybrid graphene/Si3N4 waveguides," *APL Photonics,* vol. 4, no. 7, pp. 076102, 2019/07/01, 2019.

[32] T. Gu, N. Petrone, J. F. McMillan, A. van der Zande, M. Yu, G. Q. Lo, D. L. Kwong, J. Hone, and C. W. Wong, "Regenerative oscillation and four-wave mixing in graphene optoelectronics," *Nature Photonics,* vol. 6, no. 8, pp. 554-559, 2012/08/01, 2012.

[33] M. Ji, H. Cai, L. Deng, Y. Huang, Q. Huang, J. Xia, Z. Li, J. Yu, and Y. Wang, "Enhanced parametric frequency conversion in a compact silicon-graphene microring resonator," *Optics express,* vol. 23, no. 14,18679-18685, 2015.

[34] X. Xu, J. Wu, T. G. Nguyen, M. Shoeiby, S. T. Chu, B. E. Little, R. Morandotti, A. Mitchell, and D. J. Moss, "Advanced RF and microwave functions based on an integrated optical frequency comb source," *Optics Express,* vol. 26, no. 3, pp. 2569-2583, 2018.

[35] X. Xu, J. Wu, M. Shoeiby, T. G. Nguyen, S. T. Chu, B. E. Little, R. Morandotti, A. Mitchell, and D. J. Moss, "Reconfigurable broadband microwave photonic intensity differentiator based on an integrated optical frequency comb source," *Apl Photonics,* vol. 2, no. 9, pp. 096104, 2017.

[36] H. El Dirani, A. Kamel, M. Casale, S. Kerdiles, C. Monat, X. Letartre, M. Pu, L. K. Oxenløwe, K. Yvind, and C. Sciancalepore, "Annealing-free Si3N4 frequency combs for monolithic integration with Si photonics," *Applied Physics Letters,* vol. 113, no. 8, pp. 081102, 2018/08/20, 2018.

[37] P. Demongodin, H. El Dirani, J. Lhuillier, R. Crochemore, M. Kemiche, T. Wood, S. Callard, P. Rojo-Romeo, C. Sciancalepore, C. Grillet, and C. Monat, "Ultrafast saturable absorption dynamics in hybrid graphene/Si3N4 waveguides," *APL Photonics,* vol. 4, no. 7, Jul, 2019.

[38] M. A. Foster, A. C. Turner, J. E. Sharping, B. S. Schmidt, M. Lipson, and A. L. Gaeta, "Broad-band optical parametric gain on a silicon photonic chip," *Nature,* vol. 441, no. 7096, pp. 960-3, Jun 22, 2006.

[39] T. Jiang, D. Huang, J. Cheng, X. Fan, Z. Zhang, Y. Shan, Y. Yi, Y. Dai, L. Shi, K. Liu, C. Zeng, J. Zi, J. E. Sipe, Y.-R. Shen, W.-T. Liu, and S. Wu, "Gate-tunable third-order nonlinear optical response of massless Dirac fermions in graphene," *Nature Photonics,* vol. 12, no. 7, pp. 430-436, 2018/07/01, 2018.

[40] M. Kues, C. Reimer, P. Roztocki, L. R. Cortés, S. Sciara, B. Wetzel, Y. Zhang, A. Cino, S. T. Chu, and B. E. Little, "On-chip generation of high-dimensional entangled quantum states and their coherent control," *Nature,* vol. 546, no. 7660, pp. 622-626, 2017.

[41] C. Reimer, M. Kues, P. Roztocki, B. Wetzel, F. Grazioso, B. E. Little, S. T. Chu, T. Johnston, Y. Bromberg, and L. Caspani, "Generation of multiphoton entangled quantum states by means of integrated frequency combs," *Science,* vol. 351, no. 6278, pp. 1176-1180, 2016.

[42] Y. Zhang, J. Wu, Y. Qu, L. Jia, B. Jia, and D. J. Moss, "Design and optimization of four-wave mixing in microring resonators integrated with 2D graphene oxide films", Journal of Lightwave Technology Vol. 39, (20) 6553-6562 (2021). DOI:10.1109/JLT.2021.3101292.

[43] Y. Zhang, J. Wu, Y. Qu, L. Jia, B. Jia, and D. J. Moss, "Optimizing the Kerr nonlinear optical performance of silicon waveguides integrated with 2D graphene oxide films", Journal of Lightwave Technology Vol. 39, (14) 4671-4683 (2021). DOI: 10.1109/JLT.2021.3069733.

[44] Y. Qu, J. Wu, Y. Zhang, Y. Liang, B. Jia, and D. J. Moss, "Analysis of four-wave mixing in silicon nitride waveguides integrated with 2D layered graphene oxide films", Journal of Lightwave Technology Vol. 39 (9) 2902-2910 (2021). DOI: 10.1109/JLT.2021.3059721.

[45] Y. Zhang, Y. Qu, J. Wu, L. Jia, Y. Yang, X. Xu, B. Jia, and D. J. Moss, "Graphene oxide for enhanced nonlinear optics in silicon and other CMOS compatible platforms", Paper IW1A.1, Integrated Photonics Research, Silicon and Nanophotonics, OSA Advanced Photonics Congress, Montreal, Canada, 26 – 29 July (2021).

[46] Y. Zhang, J. Wu, Y. Yang, Y. Qu, L. Jia, Y. Liang, H. El Dirani, R. Crochemore, P. Demongodinc, C. Sciancalepore, C. Grillet, C. Monat,B. Jia, and D. J. Moss, "Enhanced Kerr nonlinear performance in graphene oxide-coated silicon and silicon nitride waveguides", Paper SF2O.7, Conf. for Lasers and Electro-Optics, San Jose CA, May 9 - 14 (2021).

[47] Y. Qu, J. Wu, Y. Zhang, L. Jia, Y. Yang, X. Xu, S. T. Chu, B. E. Little, R. Morandotti, B. Jia, and D. J. Moss, "Graphene oxide for enhanced optical nonlinear performance in CMOS compatible integrated devices", Paper 11688-30, PW21O-OE109-36, 2D Photonic Materials and Devices IV, SPIE Photonics West, San Francisco CA March 6 -11 (2021). doi.org/10.1117/12.2583978

[48] L. Jia, J. Wu, Y. Zhang, Y. Qu, B. Jia, Z. Chen, and D. J. Moss, "Fabrication Technologies for the On-Chip Integration of 2D Materials", Small: Methods, Vol. 6, 2101435 (2022). DOI:10.1002/smtd.202101435.

[49] X. Xu et al, "Photonic perceptron based on a Kerr microcomb for scalable high speed optical neural networks", Laser and Photonics Reviews, vol. 14, no. 8, 2000070 (2020). DOI: 10.1002/lpor.202000070.

[50] X. Xu, et al., "11 TOPs photonic convolutional accelerator for optical neural networks", Nature **589**, 44-51 (2021).

[51] Feldmann, J. *et al.*, "Parallel convolutional processing using an integrated photonic tensor core", Nature **589**, 52-58 (2021).

[52] T. Zhou et al, "Large-scale neuromorphic optoelectronic computing with a reconfigurable diffractive processing unit", Nature Photonics Vol 15, (5) 367 (2021).

[53] B. J. Shastri *et al.,* "Photonics for artificial intelligence and neuromorphic computing", Nature Photonics **15,** (2) 102-114 (2021).

[54] Tait, A. N. et al., "Demonstration of WDM weighted addition for principal component analysis", Optics Express **23**, 12758-12765 (2015).

[55] Pasquazi, A. et al. Micro-combs: a novel generation of optical sources. Physics Reports **729**, 1-81 (2018).

[56] Moss, D. J. et al., "New CMOS-compatible platforms based on silicon nitride and Hydex for nonlinear optics", Nature photonics **7**, 597 (2013).

[57] Kippenberg, T. J., Gaeta, A. L., Lipson, M. & Gorodetsky, M. L. Dissipative Kerr solitons in optical microresonators. Science **361**, 567 (2018).

[58] Savchenkov, A. A. et al. Tunable optical frequency comb with a crystalline whispering gallery mode resonator. Physics Review Letters **101**, 093902 (2008).

[59] Spencer, D. T. et al. An optical-frequency synthesizer using integrated photonics. Nature **557**, 81-85 (2018).

[60] Marin-Palomo, P. et al. Microresonator-based solitons for massively parallel coherent optical communications. Nature **546**, 274 (2017).

[61] B. Corcoran, et al., "Ultra-dense optical data transmission over standard fiber with a single chip source", Nature Communications, vol. 11, Article:2568, 2020.

[62] Kues, M. et al. Quantum optical microcombs. Nature Photonics **13**, (3) 170-179 (2019). doi:10.1038/s41566-019-0363-0

[63] C. Reimer, L. Caspani, M. Clerici, et al., "Integrated frequency comb source of heralded single photons," Optics Express, vol. 22, no. 6, pp. 6535-6546, 2014.

[64] C. Reimer, et al., "Cross-polarized photon-pair generation and bi-chromatically pumped optical parametric oscillation on a chip", Nature Communications, vol. 6, Article 8236, 2015. DOI: 10.1038/ncomms9236.

[65] L. Caspani, C. Reimer, M. Kues, et al., "Multifrequency sources of quantum correlated photon pairs on-chip: a path toward integrated Quantum Frequency Combs," Nanophotonics, vol. 5, no. 2, pp. 351-362, 2016.

[66] C. Reimer et al., "Generation of multiphoton entangled quantum states by means of integrated frequency combs," Science, vol. 351, no. 6278, pp. 1176-1180, 2016.

[67] M. Kues, et al., "On-chip generation of high-dimensional entangled quantum states and their coherent control", Nature, vol. 546, no. 7660, pp. 622-626, 2017.

[68] P. Roztocki et al., "Practical system for the generation of pulsed quantum frequency combs," Optics Express, vol. 25, no. 16, pp. 18940-18949, 2017.

[69] Y. Zhang, et al., "Induced photon correlations through superposition of two four-wave mixing processes in integrated cavities", Laser and Photonics Reviews, vol. 14, no. 7, pp. 2000128, 2020. DOI: 10.1002/lpor.202000128

[70] C. Reimer, et al.,"High-dimensional one-way quantum processing implemented on d-level cluster states", Nature Physics, vol. 15, no.2, pp. 148–153, 2019.

[71] Stern, B., Ji, X., Okawachi, Y., Gaeta, A. L. & Lipson, M. Battery-operated integrated frequency comb generator. Nature **562**, 401 (2018).

[72] H. Bao, et al., Laser cavity-soliton microcombs, Nature Photonics, vol. 13, no. 6, pp. 384-389, Jun. 2019.

[73] Lugiato, L. A., Prati, F. & Brambilla, M. Nonlinear Optical Systems, (Cambridge University Press, 2015).

[74] Cole, D. C., Lamb, E. S., Del'Haye, P., Diddams, S. A. & Papp, S. B. Soliton crystals in Kerr resonators. Nature Photonics **11**, 671 (2017).

[75] Wang, W., et al.., Robust soliton crystals in a thermally controlled microresonator, Opt. Lett., 43, 2002 (2018).

[76] Bao, C., et al., Direct soliton generation in microresonators, Opt. Lett, **42**, 2519 (2017).

[77] M.Ferrera et al., "CMOS compatible integrated all-optical RF spectrum analyzer", Optics Express, vol. 22, no. 18, 21488 - 21498 (2014).

[78] A. Pasquazi, et al., "Sub-picosecond phase-sensitive optical pulse characterization on a chip", Nature Photonics, vol. 5, no. 10, pp. 618-623 (2011).

[79] M. Kues, et al., "Passively modelocked laser with an ultra-narrow spectral width", Nature Photonics, vol. 11, no. 3, pp. 159, 2017.

[80] L. Razzari, et al., "CMOS-compatible integrated optical hyper-parametric oscillator," Nature Photonics, vol. 4, no. 1, pp. 41-45, 2010.

[81] M. Ferrera, et al., "Low-power continuous-wave nonlinear optics in doped silica glass integrated waveguide structures," Nature Photonics, vol. 2, no. 12, pp. 737-740, 2008.

[82] M.Ferrera et al."On-Chip ultra-fast 1st and 2nd order CMOS compatible all-optical integration", Opt. Express, vol. 19, (23)pp. 23153-23161 (2011).

[83] D. Duchesne, M. Peccianti, M. R. E. Lamont, et al., "Supercontinuum generation in a high index doped silica glass spiral waveguide," Optics Express, vol. 18, no, 2, pp. 923-930, 2010.

[84] H Bao, L Olivieri, M Rowley, ST Chu, BE Little, R Morandotti, DJ Moss, ... "Turing patterns in a fiber laser with a nested microresonator: Robust and controllable microcomb generation", Physical Review Research **2** (2), 023395 (2020).

[85] M. Ferrera, et al., "On-chip CMOS-compatible all-optical integrator", Nature Communications, vol. 1, Article 29, 2010.

[86] A. Pasquazi, et al., "All-optical wavelength conversion in an integrated ring resonator," Optics Express, vol. 18, no. 4, pp. 3858-3863, 2010.

[87] A. Pasquazi, Y. Park, J. Azana, et al., "Efficient wavelength conversion and net parametric gain via Four Wave Mixing in a high index doped silica waveguide," Optics Express, vol. 18, no. 8, pp. 7634-7641, 2010.
[88] M. Peccianti, M. Ferrera, L. Razzari, et al., "Subpicosecond optical pulse compression via an integrated nonlinear chirper," Optics Express, vol. 18, no. 8, pp. 7625-7633, 2010.
[89] Little, B. E. et al., "Very high-order microring resonator filters for WDM applications", IEEE Photonics Technol. Lett. **16**, 2263–2265 (2004).
[90] M. Ferrera et al., "Low Power CW Parametric Mixing in a Low Dispersion High Index Doped Silica Glass Micro-Ring Resonator with Q-factor > 1 Million", Optics Express, vol.17, no. 16, pp. 14098–14103 (2009).
[91] M. Peccianti, et al., "Demonstration of an ultrafast nonlinear microcavity modelocked laser", Nature Communications, vol. 3, pp. 765, 2012.
[92] A. Pasquazi, et al., "Self-locked optical parametric oscillation in a CMOS compatible microring resonator: a route to robust optical frequency comb generation on a chip," Optics Express, vol. 21, no. 11, pp. 13333-13341, 2013.
[93] A. Pasquazi, et al., "Stable, dual mode, high repetition rate mode-locked laser based on a microring resonator," Optics Express, vol. 20, no. 24, pp. 27355-27362, 2012.
[94] Wu, J. *et al.* RF Photonics: An Optical Microcombs' Perspective. IEEE Journal of Selected Topics in Quantum Electronics Vol. **24**, 6101020, 1-20 (2018).
[95] Xu, X., et al., Photonic microwave true time delays for phased array antennas using a 49 GHz FSR integrated micro-comb source, *Photonics Research*, **6**, B30-B36 (2018).
[96] T. G. Nguyen *et al.*, "Integrated frequency comb source-based Hilbert transformer for wideband microwave photonic phase analysis," *Opt. Express*, vol. 23, no. 17, pp. 22087-22097, Aug. 2015.
[97] X. Xu, J. Wu, M. Shoeiby, T. G. Nguyen, S. T. Chu, B. E. Little, R. Morandotti, A. Mitchell, and D. J. Moss, "Reconfigurable broadband microwave photonic intensity differentiator based on an integrated optical frequency comb source," *APL Photonics*, vol. 2, no. 9, 096104, Sep. 2017.
[98] X. Xu, M. Tan, J. Wu, R. Morandotti, A. Mitchell, and D. J. Moss, "Microcomb-based photonic RF signal processing", *IEEE Photonics Technology Letters*, vol. 31 no. 23 1854-1857, 2019.
[99] X. Xu, *et al.*, "Broadband RF channelizer based on an integrated optical frequency Kerr comb source," *Journal of Lightwave Technology*, vol. 36, no. 19, pp. 4519-4526, 2018.
[100] X. Xu, *et al.*, "Continuously tunable orthogonally polarized RF optical single sideband generator based on micro-ring resonators," *Journal of Optics*, vol. 20, no. 11, 115701. 2018.
[101] X. Xu, *et al.*, "Orthogonally polarized RF optical single sideband generation and dual-channel equalization based on an integrated microring resonator," *Journal of Lightwave Technology*, vol. 36, no. 20, pp. 4808-4818. 2018.
[102] M.Tan, X. Xu, J. Wu, B. Corcoran, A. Boes, T. G. Nguyen, Sai T. Chu, B. E. Little, R.Morandotti, A. Mitchell, and D. J. Moss, "Integral order photonic RF signal processors based on a soliton crystal micro-comb source", IOP Journal of Optics vol. 23 (11) 125701 (2021).
[103] X. Xu, *et al.*, "Advanced adaptive photonic RF filters with 80 taps based on an integrated optical micro-comb source," *Journal of Lightwave Technology*, vol. 37, no. 4, pp. 1288-1295, 2019.
[104] X. Xu, *et al.,* Broadband microwave frequency conversion based on an integrated optical micro-comb source", *Journal of Lightwave Technology*, vol. 38 no. 2, pp. 332-338, 2020.
[105] M. Tan, *et al.*, "Photonic RF and microwave filters based on 49GHz and 200GHz Kerr microcombs", *Optics Comm*. vol. 465,125563, Feb. 22. 2020.
[106] X. Xu, *et al.,* "Broadband photonic RF channelizer with 90 channels based on a soliton crystal microcomb", *Journal of Lightwave Technology*, Vol. 38, no. 18, pp. 5116 - 5121, 2020. doi: 10.1109/JLT.2020.2997699.
[107] X. Xu, *et al.,* "Photonic RF and microwave integrator with soliton crystal microcombs", *IEEE Transactions on Circuits and Systems II: Express Briefs*, vol. 67, no. 12, pp. 3582-3586, 2020. DOI:10.1109/TCSII.2020.2995682.
[108] X. Xu, *et al.,* "Photonic RF phase-encoded signal generation with a microcomb source", *J. Lightwave Technology*, vol. 38, no. 7, 1722-1727, 2020.
[109] X. Xu, *et al.,* "High performance RF filters via bandwidth scaling with Kerr micro-combs," *APL Photonics*, vol. 4, no. 2, pp. 026102. 2019.
[110] M. Tan, *et al.*, "Microwave and RF photonic fractional Hilbert transformer based on a 50 GHz Kerr micro-comb", *Journal of Lightwave Technology*, vol. 37, no. 24, pp. 6097 – 6104, 2019.
[111] M. Tan, *et al.*, "RF and microwave fractional differentiator based on photonics", *IEEE Transactions on Circuits and Systems: Express Briefs*, vol. 67, no.11, pp. 2767-2771, 2020. DOI:10.1109/TCSII.2020.2965158.
[112] M. Tan, *et al*., "Photonic RF arbitrary waveform generator based on a soliton crystal micro-comb source", Journal of Lightwave Technology, vol. 38, no. 22, pp. 6221-6226, Oct 22. 2020. DOI: 10.1109/JLT.2020.3009655.

[113] M. Tan, X. Xu, J. Wu, R. Morandotti, A. Mitchell, and D. J. Moss, "RF and microwave high bandwidth signal processing based on Kerr Micro-combs", Advances in Physics X, VOL. 6, NO. 1, 1838946 (2021). DOI:10.1080/23746149.2020.1838946.
[114] X. Xu, et al., "Advanced RF and microwave functions based on an integrated optical frequency comb source," Opt. Express, vol. 26 (3) 2569 2018.
[115] Kues, M. et al. Quantum optical microcombs. Nature Photonics **13**, (3) 170-179 (2019). doi:10.1038/s41566-019-0363-0
[116] P.Roztocki et al., "Complex quantum state generation and coherent control based on integrated frequency combs", Journal of Lightwave Technology **37** (2) 338-347 (2019).
[117] S. Sciara et al., "Generation and Processing of Complex Photon States with Quantum Frequency Combs", IEEE Photonics Technology Letters **31** (23) 1862-1865 (2019). DOI: 10.1109/LPT.2019.2944564.
[118] L. Caspani, C. Reimer, M. Kues, et al., "Multifrequency sources of quantum correlated photon pairs on-chip: a path toward integrated Quantum Frequency Combs," Nanophotonics, vol. 5, no. 2, pp. 351-362, 2016.
[119] C. Reimer et al., "Generation of multiphoton entangled quantum states by means of integrated frequency combs," Science, vol. 351, no. 6278, pp. 1176-1180, 2016.
[120] M. Kues, et al., "On-chip generation of high-dimensional entangled quantum states and their coherent control", Nature, vol. 546, no. 7660, pp. 622-626, 2017.
[121] P. Roztocki et al., "Practical system for the generation of pulsed quantum frequency combs," Optics Express, vol. 25, no.16, 18940-18949, 2017.
[122] Y. Zhang, et al., "Induced photon correlations through superposition of two four-wave mixing processes in integrated cavities", Laser and Photonics Reviews, vol. 14, no. 7, pp. 2000128, 2020. DOI: 10.1002/lpor.202000128
[123] C. Reimer, et al.,"High-dimensional one-way quantum processing implemented on d-level cluster states", Nature Physics, vol. 15 (2) 148 (2019).
[124] H. Bao, et al., Laser cavity-soliton microcombs, Nature Photonics, vol. 13, no. 6, pp. 384-389, Jun. 2019.
[125] Bao, C., et al., Direct soliton generation in microresonators, Opt. Lett, **42**, 2519 (2017).
[126] M. Ferrera et al., "CMOS compatible integrated all-optical RF spectrum analyzer", Optics Express, vol. 22, (18) 21488 (2014).
[127] A. Pasquazi, et al., "Sub-picosecond phase-sensitive optical pulse characterization on a chip", Nature Photonics, vol. 5, no. 10, pp. 618-623 (2011).
[128] M. Kues, et al., "Passively modelocked laser with an ultra-narrow spectral width", Nature Photonics, vol. 11, no. 3, pp. 159, 2017.
[129] L. Razzari, et al., "CMOS-compatible integrated optical hyper-parametric oscillator," Nature Photonics, vol. 4, no. 1, 41-45, 2010.
[130] M. Ferrera, et al., "Low-power continuous-wave nonlinear optics in doped silica glass integrated waveguide structures," Nature Photonics, vol. 2, no. 12, pp. 737-740, 2008.
[131] M.Ferrera et al."On-Chip ultra-fast 1st and 2nd order CMOS compatible all-optical integration", Opt. Express, vol. 19, (23)pp. 23153-23161 (2011).
[132] D. Duchesne, M. Peccianti, M. R. E. Lamont, et al., "Supercontinuum generation in a high index doped silica glass spiral waveguide," Optics Express, vol. 18, no, 2, pp. 923-930, 2010.
[133] H Bao, L Olivieri, M Rowley, ST Chu, BE Little, R Morandotti, DJ Moss, ... "Turing patterns in a fiber laser with a nested microresonator: Robust and controllable microcomb generation", Physical Review Research **2** (2), 023395 (2020).
[134] M. Ferrera, et al., "On-chip CMOS-compatible all-optical integrator", Nature Communications, vol. 1, Article 29, 2010.
[135] A. Pasquazi, et al., "All-optical wavelength conversion in an integrated ring resonator," Optics Express, vol. 18 (4) 3858 (2010).
[136] A. Pasquazi, Y. Park, J. Azana, et al., "Efficient wavelength conversion and net parametric gain via Four Wave Mixing in a high index doped silica waveguide," Optics Express, vol. 18, no. 8, pp. 7634-7641, 2010.
[137] M. Peccianti, M. Ferrera, L. Razzari, et al., "Subpicosecond optical pulse compression via an integrated nonlinear chirper," Optics Express, vol. 18, no. 8, pp. 7625-7633, 2010.
[138] Little, B. E. et al., "Very high-order microring resonator filters for WDM applications", IEEE Phot. Technol. Lett. **16**, 2263(2004).
[139] M. Ferrera et al., "Low Power CW Parametric Mixing in a Low Dispersion High Index Doped Silica Glass Micro-Ring Resonator with Q-factor > 1 Million", Optics Express, vol.17, no. 16, pp. 14098–14103 (2009).
[140] M. Peccianti, et al., "Demonstration of an ultrafast nonlinear microcavity modelocked laser", Nature Comm., vol. 3, 765, 2012.

[141] A. Pasquazi, et al., "Self-locked optical parametric oscillation in a CMOS compatible microring resonator: a route to robust optical frequency comb generation on a chip," Optics Express, vol. 21, no. 11, pp. 13333-13341, 2013.
[142] A. Pasquazi, et al., "Stable, dual mode, high repetition rate mode-locked laser based on a microring resonator," Optics Express, vol. 20, no. 24, pp. 27355-27362, 2012.
[143] Xu, X., et al., Photonic microwave true time delays for phased array antennas using a 49 GHz FSR integrated micro-comb source, *Photonics Research*, **6**, B30-B36 (2018).
[144] X. Xu, M. Tan, J. Wu, R. Morandotti, A. Mitchell, and D. J. Moss, "Microcomb-based photonic RF signal processing", *IEEE Photonics Technology Letters*, vol. 31 no. 23 1854-1857, 2019.
[145] M. Tan et al, "Orthogonally polarized Photonic Radio Frequency single sideband generation with integrated micro-ring resonators", IOP Journal of Semiconductors, Vol. **42** (4), 041305 (2021). DOI: 10.1088/1674-4926/42/4/041305.
[146] Xu, *et al.*, "Advanced adaptive photonic RF filters with 80 taps based on an integrated optical micro-comb source," *Journal of Lightwave Technology*, vol. 37, no. 4, pp. 1288-1295 (2019).
[147] X. Xu, *et al.,* Broadband microwave frequency conversion based on an integrated optical micro-comb source", *Journal of Lightwave Technology*, vol. 38 no. 2, pp. 332-338, 2020.
[148] M. Tan, *et al.,* "Photonic RF and microwave filters based on 49GHz and 200GHz Kerr microcombs", *Optics Comm*. vol. 465,125563, Feb. 22. 2020.
[149] X. Xu, *et al.,* "Broadband photonic RF channelizer with 90 channels based on a soliton crystal microcomb", *Journal of Lightwave Technology*, Vol. 38, no. 18, pp. 5116 - 5121, 2020. doi: 10.1109/JLT.2020.2997699.
[150] X. Xu, *et al.,* "Photonic RF and microwave integrator with soliton crystal microcombs", *IEEE Transactions on Circuits and Systems II: Express Briefs*, vol. 67, no. 12, pp. 3582-3586, 2020. DOI:10.1109/TCSII.2020.2995682.
[151] X. Xu, *et al.,* "High performance RF filters via bandwidth scaling with Kerr micro-combs," *APL Photonics,* vol. 4 (2) 026102. 2019.
[152] M. Tan, *et al.,* "Microwave and RF photonic fractional Hilbert transformer based on a 50 GHz Kerr micro-comb", *Journal of Lightwave Technology*, vol. 37, no. 24, pp. 6097 – 6104, 2019.
[153] M. Tan, *et al.,* "RF and microwave fractional differentiator based on photonics", *IEEE Transactions on Circuits and Systems: Express Briefs*, vol. 67, no.11, pp. 2767-2771, 2020. DOI:10.1109/TCSII.2020.2965158.
[154] M. Tan, *et al*., "Photonic RF arbitrary waveform generator based on a soliton crystal micro-comb source", Journal of Lightwave Technology, vol. 38, no. 22, pp. 6221-6226 (2020). DOI: 10.1109/JLT.2020.3009655.
[155] M. Tan, X. Xu, J. Wu, R. Morandotti, A. Mitchell, and D. J. Moss, "RF and microwave high bandwidth signal processing based on Kerr Micro-combs", Advances in Physics X, VOL. 6, NO. 1, 1838946 (2021). DOI:10.1080/23746149.2020.1838946.
[156] X. Xu, et al., "Advanced RF and microwave functions based on an integrated optical frequency comb source," Opt. Express, vol. 26 (3) 2569 (2018).
[157] M. Tan, X. Xu, J. Wu, B. Corcoran, A. Boes, T. G. Nguyen, S. T. Chu, B. E. Little, R.Morandotti, A. Lowery, A. Mitchell, and D. J. Moss, ""Highly Versatile Broadband RF Photonic Fractional Hilbert Transformer Based on a Kerr Soliton Crystal Microcomb", Journal of Lightwave Technology vol. 39 (24) 7581-7587 (2021).
[158] Bao, C., et al., Direct soliton generation in microresonators, Opt. Lett, 42, 2519 (2017).
[159] Yuning Zhang, Yang Qu, Jiayang Wu, Linnan Jia, Yunyi Yang, Xingyuan Xu, Baohua Jia, and David J. Moss, "Enhanced Kerr nonlinearity and nonlinear figure of merit in silicon nanowires integrated with 2D graphene oxide films", ACS Applied Materials and Interfaces, Vol. 12 (29) 33094−33103 (2020). DOI:10.1021/acsami.0c07852
[160] D.Moss, "11 Tera-FLOP/s photonic convolutional accelerator and deep learning optical neural networks", Research Square, (2021). DOI: https://doi.org/10.21203/rs.3.rs-493347/v1.
[161] Moss, David (2020): "11.0 Tera-FLOP/second photonic convolutional accelerator for deep learning optical neural networks", TechRxiv. Preprint. (2020). https://doi.org/10.36227/techrxiv.13238423.v1
[162] Xu, X.; Tan, M.; Corcoran, B.; Wu, J.; Boes, A.; Nguyen, T.; Chu, S.; Little, B.; Hicks, D.; Morandotti, R.; Mitchell, A.; Moss, D. "11 Tera-FLOP per Second Photonic Convolutional Accelerator for Deep Learning Optical Neural Networks", Preprints 2020, 2020110420.
[163] Moss, David (2020): "RF and microwave photonic high bandwidth signal processing based on Kerr micro-comb sources", TechRxiv. (2020). Preprint. DOI:10.36227/techrxiv.12665609.v3
[164] Yuning Zhang, Jiayang Wu, Yunyi Yang, Yang Qu, Linnan Jia, Tania Moein, Baohua Jia, David J. Moss, "Enhanced nonlinear optical figure-of-merit at 1550nm for silicon nanowires integrated with graphene oxide layered films", Arxiv (2020). arXiv:2004.08043 [physics.optics]
[165] Moss, David; Jia, Baohua; Wu, Jiayang; Zhang, Yuning; Yang, Yunyi; Jia, Linnan, Yang Qu, Tania Moein (2020): "Transforming silicon into a high performing integrated nonlinear photonics platform by integration with 2D graphene oxide films", TechRxiv. (2020). Preprint. DOI:10.36227/techrxiv.12061809.v1.

[166] A. Frigg, A. Boes, G. Ren, T.G. Nguyen, D.Y. Choi, S. Gees, D. Moss, A Mitchell, “Optical frequency comb generation with low temperature reactive sputtered silicon nitride waveguides”, APL Photonics, Vol. 5 (1), 011302 (2020).

[167] T. Moein, D. Gailevičius, T. Katkus, S.H. Ng, S. Lundgaard, D.J. Moss, H. Kurt, Vygantas Mizeikis, Kęstutis Staliūnas, Mangirdas Malinauskas, Saulius Juodkazis, “Optically-thin broadband graphene-membrane photodetector”, Nanomaterials, Vol. 10 (3), 407 (2020).

[168] M. Tan, X. Xu, J. Wu, A. Boes, B. Corcoran, T. G. Nguyen, S. T. Chu, B. E. Little, R. Morandotti, A. Mitchell, and D. J. Moss, “Advanced applications of Kerr mircocombs”, Paper 11775-1. SPIE 11775, Integrated Optics: Design, Devices, Systems and Applications VI, (EOO21) OO107-8, Proc 1177504 (18 April 2021); Integrated Optics Conference, SPIE Optics and Optoelectronics Symposium, Prague, Czech Republic. April 19 - 22 (2021), doi.org/10.1117/12.2588733.

[169] Moss, David, “Microcombs for Ultrahigh Bandwidth Optical Data Transmission and Neural Networks.” OSF Preprints. March 8. (2021). DOI:10.31219/osf.io/ne9wx.